IMPLEMENTATION OF TOPS MODE ON RADARSAT-2 IN SUPPORT OF THE SENTINEL-1 MISSION

Gordon Davidson [(1)], Vincent Mantle [(1)], Bernhard Rabus [(1)], Dan Williams [(1)], Dirk Geudtner [(2)]

[(1)] MDA,13800 Commerce Parkway, Richmond, BC, Canada, V6V2J3
[(2)] ESA ESTEC,Keplerlaan 1, 2201 AG Noordwijk, Netherlands

ABSTRACT

TOPS is the main imaging mode on Sentinel-1 and has been implemented recently as an experimental mode on RADARSAT-2. This paper describes aspects of the beam mode design for RADARSAT-2, and presents the results of expected coherence based on statistical analysis of existing RADARAT-2 InSAR stacks. Performance results for radiometry and point target analysis are presented for the test scenes that have been acquired. Doppler grid results and initial interferometry results are also presented.

1. INTRODUCTION

The Interferometric Wide Swath (IW) mode is the main mode of operations for Sentinel-1 and will support the use of SAR Interferometry (InSAR) techniques for applications such as monitoring of surface deformation. It will operate in the new TOPS mode, which is a type of ScanSAR imaging except that the antenna is steered forward in the azimuth direction during the acquisition of a burst.

The RADARSAT-2 mission operates at the same C-band frequency as Sentinel-1, and its phased array antenna supports multiple SAR imaging modes. An experimental TOPS mode, designed to be as similar as possible to the Sentinel-1 IW mode, has been implemented on RADARSAT-2 in order to prepare for processing of and exploitation of Sentinel-1 IW data.

2. RADARSAT-2 TOPS DESIGN

2.1. TOPS Review

The TOPS imaging geometry is illustrated in Fig. 1. During each burst, the antenna is steered forward in the azimuth direction, covering an azimuth extent on the ground that overlaps with area covered by the adjacent bursts to ensure continuous coverage. The scanning of the antenna in azimuth, at a rate of k_θ rad/s, means that each target is illuminated by the entire azimuth antenna pattern, thus avoiding the scalloping associated with ScanSAR images. It also reduces the illumination time of the target by the factor

$$\alpha = 1 + \frac{k_\theta R}{v_g} \qquad (1)$$

where R is range and v_g is ground velocity, so that azimuth resolution is reduced accordingly [1]. The scanning also results in a variation in the Doppler locations of targets across the burst. This Doppler sweep rate is given by

$$k_s = \frac{2v_s}{\lambda} k_\theta \text{ Hz/s.} \qquad (2)$$

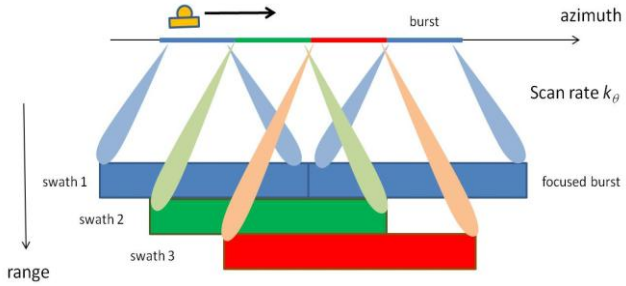

Figure 1. TOPS imaging geometry.

2.2. TOPS Design

The experimental TOPS mode is based on the existing RADARSAT-2 ScanSAR Narrow B mode, which has three sub-swaths and covers a comparable range of incidence angles. For the TOPS mode the pulse bandwidth is increased to be closer to that of Sentinel-1 IW. A comparison of basic mode parameters of RADARSAT-2 TOPS and Sentinel-1 IW is shown in Tab. 1 [3].

Table 1. Comparison of RADARSAT-2 TOPS and Sentinel-1 mode parameters.

	RTOPS	Sentinel-1 IW
Number of swaths	3	3
Ground range coverage, km	284	251
Incidence angle, degrees	31.3 – 46.5	30.0 – 45.1
Nominal slant range resolution, m	5.0	2.7 / 3.1 / 3.5
Nominal azimuth resolution, m	29	21

The expected values for NESZ in RADARSAT-2 TOPS are from the three beams that make up each of the sub-swaths in the RADARSAT-2 ScanSAR Narrow B mode, adjusted for the different pulse bandwidth. The NESZ for RADARSAT-2 TOPS is compared with the expected values for Sentinel in Fig. 2.

Proc. 'ESA Living Planet Symposium 2013', Edinburgh, UK
9–13 September 2013 (ESA SP-722, December 2013)

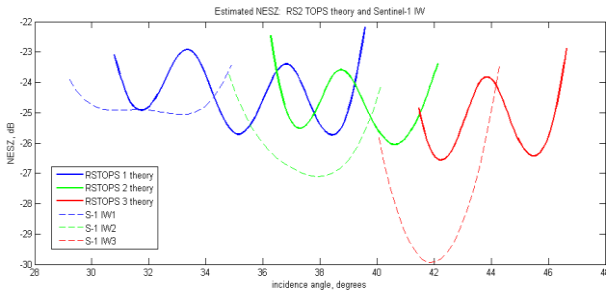

Fig 2. Comparison of NESZ for RADARSAT-2 TOPS and Sentinel-1.

The azimuth scanning required for TOPS mode was designed to be close to that of Sentinel-1. The burst durations and the azimuth angle beam steering limits per burst are chosen to be approximately the same as those of Sentinel-1. One difference is that RADARSAT-2 can only steer the antenna in coarse steps. The step size is limited by the minimum beam switching time, which an in-orbit experiment found to be about 15 ms. The step size is also limited by the number of Timing Control patterns that can be uploaded to the satellite. This sets a limit on the total number of azimuth steps across all sub-swaths, which for a certain maximum pointing angle limits the step size. The step size in azimuth antenna steering for RADARSAT-2 TOPS is 0.03975 degrees. Other TOPS design parameters, shown as averages across sub-swaths, are compared for RADARSAT-2 TOPS and Sentinel-1 in Tab. 2.

Table 2. Comparison of RADARSAT-2 and Sentinel-1 TOPS design parameters.

	Average RTOPS	Average Sentinel-1
Step size, degrees	0.03975	0.0016
Max azimuth pointing angle per burst, deg	0.56	0.55
Burst duration, sec	1.02	0.9
Scan rate, deg/s	1.13	1.25
Doppler rate due to scan, Hz/s	5341	5953
Focused burst extent, sec	3.4	2.8
Focused burst overlap, %	10	3

2.3. Effect of Coarse Step

The effect of the coarse step size is a distortion of the amplitude of the SAR signal in azimuth as shown in Fig. 3. The signal with smooth steering is shown in blue, and the signal with coarse stepped steering is shown in green. With coarse steps, the amplitude follows the non-steered azimuth antenna beam pattern during a step, and then jumps to the point along the beam pattern corresponding to the next step. In between are a number of pulses that were transmitted on the old step and received on the new one.

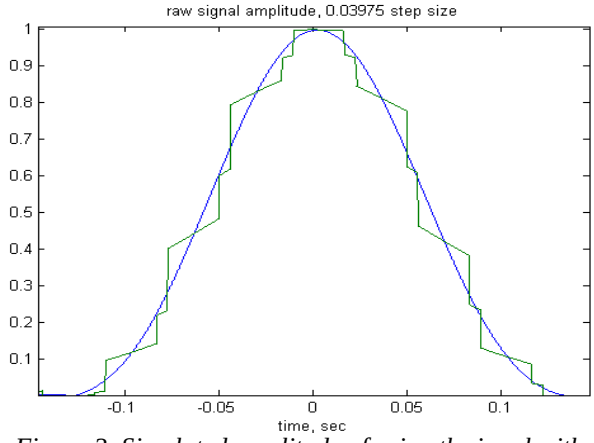

Figure 3. Simulated amplitude of azimuth signal with coarse antenna steering step size.

The distortion in the amplitude of the azimuth SAR signal has an effect on the azimuth point target response, which is shown in Fig 4. However, the effect is not severe, being approximately a 0.7 dB degradation in sidelobe level. There is also a small 0.05 dB variation in radiometry.

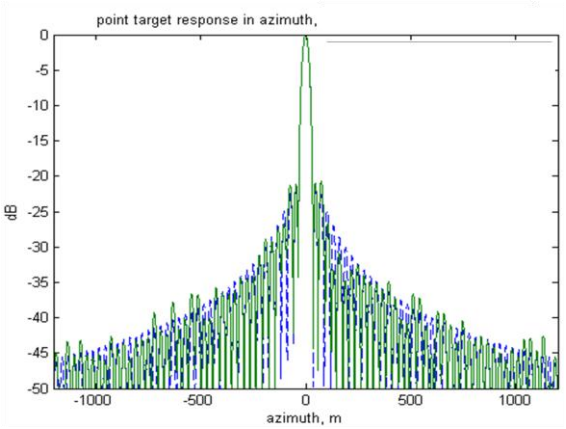

Figure4. Simulated point target response with coarse step size.

3. EXPECTED COHERENCE

The coherence of bursts from two interferometric passes is affected by the synchronization of the two bursts [2], and by a difference in Doppler centroid due to orbit and attitude. For a burst misalignment of T_{del} seconds, the azimuth spectral shift between correlated spectral components of the TOPS bursts can be shown to be

$$\Delta f_T = \frac{-k_s T_{del}}{\alpha} \quad \text{Hz} \qquad (3)$$

This can also be shown to be

$$\Delta f_T = k_a T_{del} \frac{\alpha - 1}{\alpha} \qquad (4)$$

where k_a is the azimuth FM rate. Compared to the spectal shift for ScanSAR of

$$\Delta f_T = k_a T_{del} \qquad (5)$$

it can be seen that TOPS is slightly more forgiving of burst misalignment than ScanSAR.

For a difference in Doppler centroid of Δf_{dc}, the azimuth spectral shift between correlated spectral components of the TOPS bursts can be shown to be

$$\Delta f_f = \frac{\Delta f_{dc}}{\alpha} \quad \text{Hz} \tag{6}$$

The coherence due to azimuth spectral shift is then

$$\gamma_{az} = \frac{B_a - |\Delta f_T + \Delta f_f|}{B_a} \tag{7}$$

where B_a is the processed target azimuth bandwidth in TOPS. Combined with the coherence due to the range baseline

$$\gamma_b = \frac{b_{crit} - |b_\perp|}{b_{crit}} \tag{8}$$

where b_{crit} is the critical baseline and $b_\perp$ is the perpendicular baseline , the overall coherence due to spectral shifts is

$$\gamma = \gamma_{az}\gamma_b \tag{9}$$

In order to estimate the expected coherence between bursts, a large set of existing InSAR stacks where analyzed to obtain a statistical characterization of burst synchronization, Doppler centroid difference, and perpendicular baseline. Tab. 3 shows the 50 percentile and 90 percentile values of these quantities that were obtained the analysis.

Table 3. Summary of analysis of InSAR stacks.

	50 Percentile (pairwise absolute difference)	90 Percentile (pairwise absolute difference)
Burst Synchronization	16 milli-seconds	41 milli-seconds
Doppler Centroid Variation	36 Hz	92 Hz
Perpendicular Baseline	160 meters	435 meters

The analysis of the InSAR stacks generated probability distributions of burst synchronization, Doppler centroid difference, and perpendicular baseline. Eq. 7 to 9 were then used to create a three-dimensional probability distribution for coherence. This distribution was then integrated to obtain the probability of coherence exceeding a certain value, and this result is shown in Fig. 5. The blue curve shows the effect of only azimuth spectral shifts, and the green curve shows the effect of both azimuth and range spectral shifts. From this curve it can be seen that there is a 50% chance of coherence exceeding 0.84, and a 90% chance of coherence exceeding 0.66.

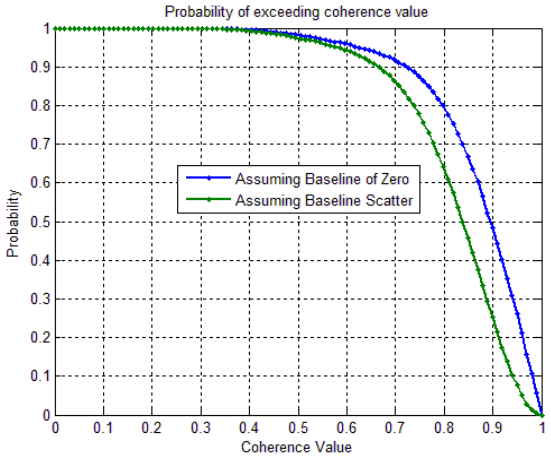

Figure 5. Probability of exceeding coherence value.

4. PROCESSING AND TEST SCENES

The processing of the acquired RADARSAT-2 TOPS data was done in the following steps.

First, the data was pre-processed with the RADARSAT-2 processor, including:

- Ingest
- Range compression
- Formatting

Next the range compressed data was used in Doppler centroid estimation. Then the range compressed data, formatted annotation data, and Doppler centroid information were input to the Sentinel-1 Instrument Processing Facility (IPF) which performed the rest of TOPS processing including

- Input range compressed data and annotation
- Upsampling
- Range cell migration correction
- Secondary range compression
- Azimuth compression
- Resampling

A number of RADARSAT-2 TOPS acquisitions were made for testing and validating various aspects of image quality, and are listed in Tab. 4.

Table 4. Test scenes.

Acqusition Date	Location	Pass Direction	Purpose
3/31/2013	Richmond, BC, Canada	Desc	IRF and DTAR measurements
4/2/2013	Amazon, Brazil	Desc	Radiometric Verification
4/10/2013	Ocean Current, Agulhas, SA	Asc	Ocean Current
4/19/2013	Ocean Current, Gulf Stream, USA	Asc	Ocean Current
5/3/2013	Montreal, Canada (CSA Transponders)	Asc	CSA St Hubert and Ottawa Transponders for IRF and location accuracy measurement.
4/1/2013	Uyuni Salt Flats, Bolivia	Asc	First image for dry area InSAR pair.
4/25/2013	Uyuni Salt Flats, Bolivia	Asc	Second image for dry area InSAR pair
4/4/2013	Mexico City	Desc	First Image for InSAR stack
4/28/2013	Mexico City	Desc	Second Image for InSAR stack
4/11/2013	Petermann Glacier, Greenland	Asc	First glacier image for InSAR pair
5/5/2013	Petermann Glacier, Greenland	Asc	Second image for glacier InSA pair.
3/28/2013	Pacific Doldrums	Asc	NESZ Estimation
3/28/2013	Istanbul, Turkey	Desc	DTAR

5. IMAGE QUALITY RESULTS

This section shows results of some image measurements that were made on the test scenes. An image of the full Richmond acquisition is shown in Fig. 6. The three sub-swaths are shown separately, and as in the RADARSAT-2 ScanSAR Narrow B mode, there is significant overlap of the sub-swaths,.

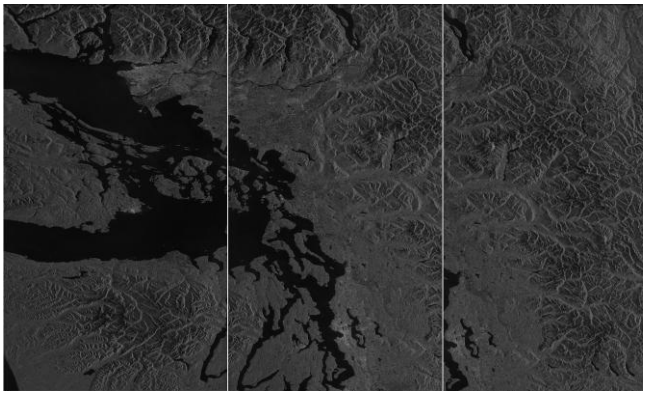

Figure 6. Processed images of three overlapping sub-swaths of Richmond acquisition.

5.1. Point Target Analysis

Point target analysis in range and azimuth was done on a target of opportunity in the Richmond image which was a barge on a river. Plots of the target response in range and azimuth are shown in Fig. 7 and 8, and the shape of the azimuth response in Fig. 8 is in close agreement with the simulated response due to the coarse step size shown in Fig. 4. Each shows the measured resolution in meters, the Integrated Sidelobe Ratio (ISLR) and Peak Sidelobe Ratio (PSLR) for the target of opportunity.

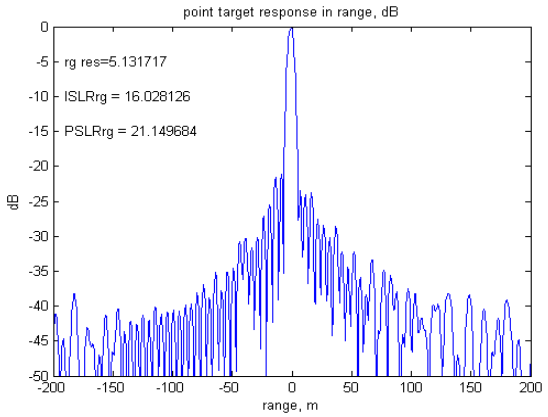

Figure 7. Point target analysis in range of target of opportunity.

The point target analysis of transponders at St. Hubert and Ottawa, in the Montreal data set, is shown in Tab. 5. The expected values for range correspond to the Hamming(0.75) weighting that was used [3]. The expected values in azimuth are determined by simulation of the effect the coarse step. The measured values are all reasonably close to the expected ones.

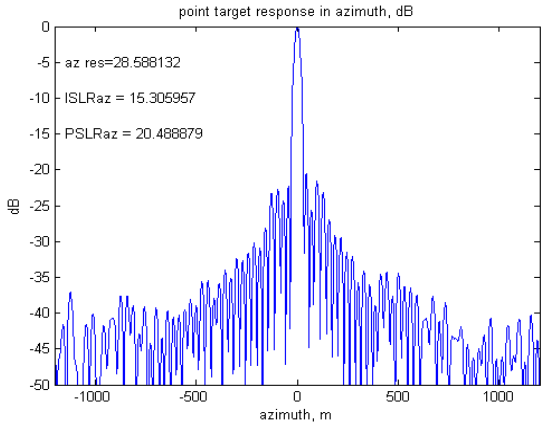

Figure 8. Point target analysis in azimuth of target of opportunity.

Table 5. Summary of point target analysis of transponders.

	Theoretical	St. Hubert	Ottawa
Range Resolution [m]	5.0	5.06	5.09
Range ISLR [dB]	-16.1	-15.62	-15.37
Range PSLR [dB]	-21.3	-21.19	-20.44
Azimuth Resolution [m]	29.4 / 29.2 / 29.0	29.08	29.50
Azimuth ISLR [dB]	-15.39	-15.37	-15.51
Azimuth PSLR [dB]	-20.66	-21.62	-20.67

5.2. Radiometry

The Amazon rainforest has a uniform γ_0 of approximately -6.5 dB, and this was used to determine output gain factors per sub-swath to apply to the processed burst images from the Amazon acquisition. Burst images were power detected, multiplied by the tangent of the incidence angle to estimate γ_0, and averaged over azimuth to form a range profile. The results for the three sub-swaths are shown in Fig. 9, which shows a stable measure of γ_0 within sub-swaths and continuity between sub-swaths.

Another aspect of radiometry is the residual scalloping due to the azimuth antenna element pattern in the electronic steering. A model for the element pattern is used to correct for the residual scalloping during processing. To verify this correction, burst images of γ_0 over the Amazon were averaged over range. The resulting azimuth profile should be flat, and the example result for sub-swath 2 shown in Fig. 10 shows that it is.

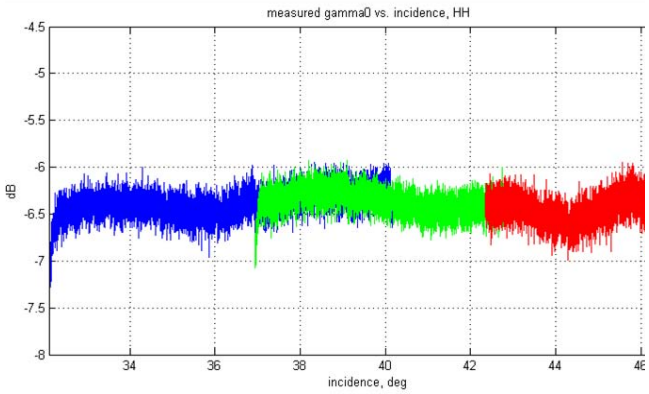

Figure 9. Profile of γ_0 vs. incidence angle for three sub-swaths over Amazon.

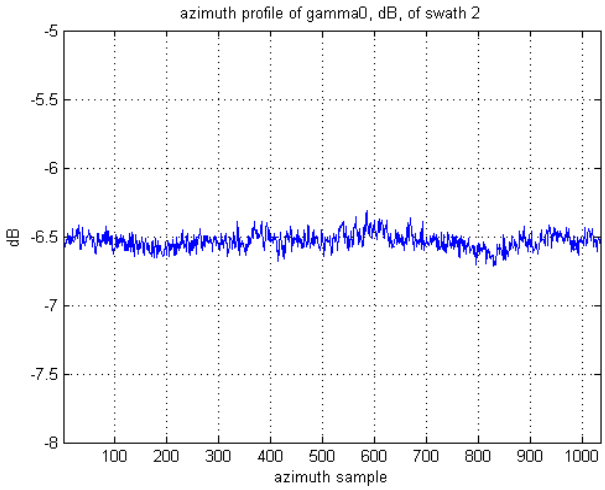

Figure 10. Azimuth profile of burst, sub-swath 2, over the Amazon.

Given the output image gains determined from the Amazon data, the Doldrums data set over very calm water was processed to estimate the Noise Equivalent Sigma Zero (NESZ). The HV data set was used which should have very low backscatter so that the output image consists of receiver noise. Power detection, multiplying by the sine of the incidence angle, and average over azimuth gives the estimates of NESZ, which are plotted vs. incidence angle for the three sub-swaths in Fig. 11. The agreement measured NESZ with the expected values is quite good.

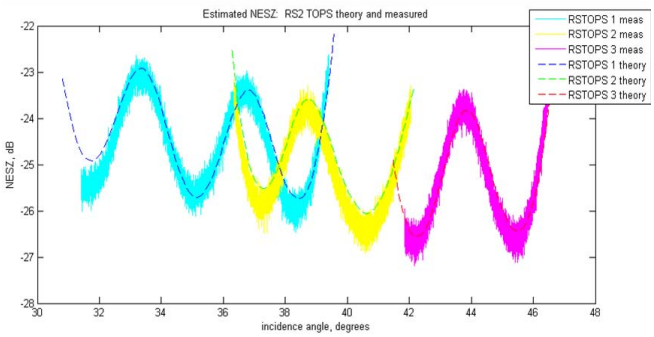

Figure 11. Measured Noise Equivalent Sigma Zero for three sub-swaths.

6. DOPPLER GRID

The Doppler grid consists of deviations from the mean of Doppler centroid estimates made from the complex SAR data. Over the ocean these measurements can be interpreted as a measure of the ocean current velocity in the line-of-sight direction. To estimate Doppler centroid within a burst, the Doppler sweep due to antenna scanning is removed by a deramp, or quadratic phase multiply, which performs an azimuth dependent, azimuth-frequency shift. To form a Doppler grid, multiple Doppler centroid estimates are made per burst

in both the range and azimuth directions. In range, 32 overlapping range segments are used per sub-swath, for a total of 96 over all 3 sub-swaths. In azimuth, 5 overlapping estimates per burst are made. The azimuth estimates have to be corrected for any small error in the Doppler sweep rate that was used to deramp the data. The results of the Doppler grid image for the Agulhas data off the coast of South Africa is shown in Fig. 12. It is shown superimposed on an ocean current map made by CLS using ASAR data during 2008, and there is good agreement between the two.

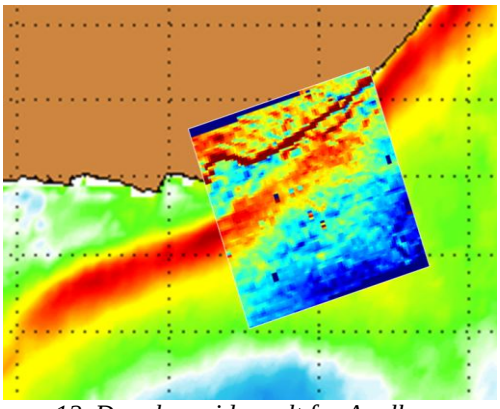

Figure 12. Doppler grid result for Agulhas current superimposed on CLS ASAR 2008 ocean current map

7. INTERFEROMETRY

Finally, burst images from two passes over the Unyui area in Bolivia were used to form interferograms and measure coherence. Registration was done by the normal correlation method, and investigations into effects of miss-registration and into mosaicking of burst interferograms are on-going.

Interferogram generation consisted of:

- Registration by the usual intensity correlation techniques
- Applying a deramp to the slave image to remove Doppler sweep due to antenna scanning
- Resampling the slave image
- Resampling the deramp function and removing it from the resampled slave image
- Common band filtering in range
- Interferogram flattening

The results for a burst in sub-swath 2 are shown in Fig. 13 to Fig 15. Fig. 13 shows the coherence which is very good across the sub-swath. Fig. 14 shows the interferometric phase, and Fig. 15 shows the interferometric phase superimposed on the amplitude image.

Figure 13. Coherence of burst, sub-swath 2, Uyuni acquisitions.

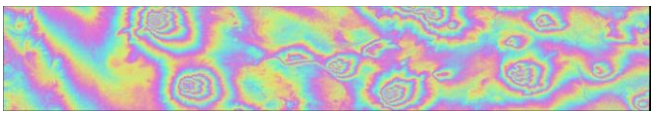

Figure 14. Interferometric phase of burst, sub- swath 2, Uyuni acquisitions.

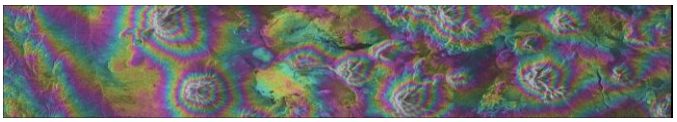

Figure 15. Interferometric phase of burst superimposed on image amplitude, sub-swath 2, Uyuni acquisitions.

8. CONCLUSION

An experimental TOPS mode has been successfully implemented on RADARSAT-2. The effect of the coarse step size is not severe. Statistical analysis of the timing of existing InSAR stacks shows good probability of coherence. Image quality results are in line with performance expectations. Doppler grid estimation was demonstrated over ocean currents. Results of interferometry show good coherence.

9. REFERENCES

1. De Zan, F., Monti Guarnieri, A. (2006). TOPSAR: Terrain Observation by Progressive Scans, *IEEE Trans. Geoscience and Remote Sensing* **44**(9), 2352–2360.
2. Monti Guarnieri, A., Prati, C., (1996). ScanSAR Focusing and Interferometry, *IEEE Trans. Geoscience and Remote Sensing* **34**(4), 1029–1037.
3. Sentinel-1 Product Definition, S1-RS-MDA-52-7440, Aug. 22, 2012.